JCI The Journal of Clinical Investigation

AAV9/MFSD8 gene therapy is effective in preclinical models of neuronal ceroid lipofuscinosis type 7 disease

Xin Chen, … , Joseph R. Mazzulli, Steven J. Gray

J Clin Invest. 2022. https://doi.org/10.1172/JCI146286.

Research In-Press Preview **Neuroscience**

Graphical abstract

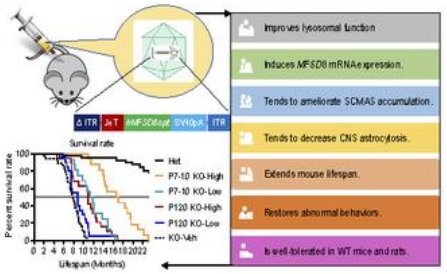

AAV9/MFSD8 gene therapy is effective in preclinical models of neuronal ceroid lipofuscinosis type 7 disease

Xin Chen[1], Thomas Dong[1], Yuhui Hu[1], Frances C. Shaffo[1], Nandkishore R. Belur[2], Joseph R. Mazzulli[2], and Steven J. Gray[1]

[1]*Department of Pediatrics, University of Texas Southwestern Medical Center, Dallas, TX 75390*

[2]*The Ken and Ruth Davee Department of Neurology, Northwestern University Feinberg School of Medicine, Chicago IL 60611*

Abstract

Neuronal ceroid lipofuscinosis type 7 (CLN7) disease is a lysosomal storage disease caused by mutations in the facilitator superfamily domain containing 8 (*MFSD8)* gene, which encodes a membrane-bound lysosomal protein MFSD8. To test the effectiveness and safety of adeno-associated viral (AAV) gene therapy, an in vitro study demonstrated that AAV2/*MFSD8* dose-dependently rescued lysosomal function in fibroblasts from a CLN7 patient. An in vivo efficacy study using intrathecal administration of AAV9/*MFSD8* to *Mfsd8*$^{-/-}$ mice at postnatal day (p)7-10 or p120 with high or low dose led to clear age- and dose-dependent effects. A high dose of AAV9/*MFSD8* at p7-10 resulted in widespread *MFSD8* mRNA expression, tendency of amelioration of subunit c of mitochondrial ATP synthase accumulation and glial fibrillary acidic protein immunoreactivity, normalization of impaired behaviors, doubled median lifespan, and extended normal body weight gain. In vivo safety studies in rodents concluded that intrathecal administration of AAV9/*MFSD8* was safe and well-tolerated. In summary, these results demonstrated that the AAV9/*MFSD8* vector is both effective and safe in preclinical models. Investigational New Drug application #19766 to initiate a Phase I intrathecal gene transfer trial for AAV9/*MFSD8* was approved by the US FDA and the trial is enrolling CLN7 patients at Children's Health in Dallas, TX in collaboration with UTSW Medical Center (clinicaltrials.gov NCT04737460).

Introduction

The variant late infantile neuronal ceroid lipofuscinosis type 7 (vLINCL7 or CLN7) disease is a lysosomal storage disease (LSD) caused by a mutation in the gene named major facilitator superfamily domain containing 8 (*MFSD8*). The *MFSD8* gene encodes a 518-amino acid polytopic lysosomal transmembrane protein with 12 membrane-spanning domains (1). Since the initial identification of a mutation in the gene in 2007, a total of 38 different *MFSD8* mutations and 2 sequence variations have been reported in populations throughout the world (2). The types of

mutations include missense, splice site, nonsense, frame shift, and sequence deletion or insertion. The autosomal recessive condition in children is inherited from healthy, carrier parents each contributing a defective allele.

Although the genetic mutations in the *MFSD8* gene resulting in CLN7 disease are well documented and the MFSD8 protein is a member of the major facilitator superfamily (MFS), the function, nature of metabolite(s) transported by MFSD8 protein (3), and therefore disease mechanisms of this progressive neurodegenerative disease are unknown. Histopathology indicates there is progressive loss in neuronal cells in the cerebral cortex layer V, complete loss of the granule cell layer in the cerebellum, age-dependent progressive losses in cerebellar Purkinje cells, and degeneration of photoreceptors in the retina (4). Loss of vision from progressive degeneration of the retina and neuroinflammation in the cerebellar and cerebral cortical regions of human patients are key features of the disease. Defective lysosomal function and dysregulation of autophagy have been suggested as potential contributors to the neurodegenerative mechanism of CLN7 disease (5, 6).

Pathobiology of the CLN7 disease is not completely understood. Human *MFSD8* mRNA is ubiquitously expressed in the central nervous system (CNS), heart, placenta, liver, skeletal muscle, and pancreas (1). *Mfsd8* mRNA is expressed throughout the rat brain, with increased levels in the granular layer of the cerebellum and pyramidal layers of the hippocampus (4). The protein is localized to lysosomal membranes (4, 5, 7, 8). MFS proteins are solute transporters and a conserved family function for the MFSD8 protein, and its localization suggests its conserved putative function as a transporter in the lysosomal membrane. Dysfunction of the MFSD8 protein results in the accumulation of lysosomal storage material or autofluorescent ceroid lipopigments in neuronal and peripheral tissues, an important feature of CLN7 disease (4, 5, 9). CLN7 patients with mutations in the *MFSD8* gene were shown to exhibit massive accumulation of subunit c of mitochondrial ATP synthase (SCMAS) in the brain and peripheral organs (10). The ultrastructure of the neuronal storage material in CLN7 patients consists of rectilinear complexes and fingerprint profiles (1, 11, 12). There is elevated expression of lysosomal proteins including *CTSD*, *CTSB*, and *CTSZ* in the CLN7 storage phenotype due to enhanced transcription (6). The buildup of storage material in CLN disease is thought to lead to the destabilization and increased permeability of the lysosomal membrane potentially resulting in apoptosis and neurodegeneration (13, 14). A common finding in LSD is a generalized neuroinflammatory response to neuronal storage as seen by astrogliosis maker glial fibrillary acidic protein (GFAP) staining (5).

The incidence and prevalence of CLN7 disease are unknown although more than 70 cases have been identified in people around the world (https://medlineplus.gov/genetics/condition/cln7-disease/#frequency). The clinical presentation of CLN7 disease can vary from a mild, late-onset presentation with non-syndromic visual deficits to a severe, early-onset version that manifest as neurological signs with progressive deterioration in intellectual and motor capabilities, seizures, muscle spasms, visual deficits culminating in premature death (1, 11, 12, 15-24). Although a recent paper reported some amelioration of CLN7 disease phenotypes by tamoxifen in cellular and

murine models (25), there is no approved treatment for patients suffering from CLN7 disease. Management of the condition is limited to symptomatic intervention to treat seizures, dystonia, anxiety, sleep disorders, and spasms (26). Surgery may be required in patients with difficulty swallowing (19). Since all aspects of CLN7 disease stem from the loss of *MFSD8* gene function, *MFSD8* gene replacement therapy represents a reasonable and promising approach to provide a meaningful and long-term therapeutic benefit for this patient population. Nevertheless, there have been no publications describing preclinical gene therapy (GT) studies for CLN7 disease.

Over the last two decades, there have been numerous viral vector-based GT approaches tested for other disorders. Collective evidence has shown that GT can be clinically therapeutic and well tolerated, resulting in therapies for rare inherited diseases and in some cases, resolving the majority of symptoms (27). Recombinant adeno-associated viral vector type 9 (AAV9) has particularly been shown to be a safe and efficacious neurotropic vector to deliver transgenes to the CNS (28). These recombinant AAV vectors are non-pathogenic, non-replicating, and transduce both dividing and non-dividing cells. Importantly, they are incapable of coding viral proteins and are primarily non-integrating, making them an ideal vector for gene delivery to the CNS (29). AAV9 mediates broad gene transfer across the entire CNS in a way that translates from mice to larger animal models (28-38). Furthermore, AAV9 can be purified in large quantities at high concentrations for potential use in delivering a functional copy of a gene to cells with aberrant, disease causing mutations directly to the CNS using intrathecal (IT) administration (28-38). AAV9 is also the vector utilized in the US Food and Drug Administration (FDA)-approved GT by an intravenous (IV) route, Zolgensma®, for infants with spinal muscular atrophy (SMA). The AAV9 vector is also being used for ongoing GT clinical trials including an AAV9 vector for Giant Axonal Neuropathy (GAN) that was developed by our group and is being used in the first human IT-administered AAV trial at the US National Institutes of Health (NIH) Clinical Center (30).

In this study, we utilized an approach similar to GAN GT to evaluate the efficacy and safety of *MFSD8* gene transfer in vitro in fibroblasts from a CLN7 patient as well as in KO mouse models to investigate whether this would show a potential benefit to pediatric patients suffering from CLN7 disease. To inform the relative risks associated with this approach, we conducted a dose-ranging, 1-year non-good laboratory practice (GLP) toxicology study in WT C57BL/6J mice by IT administration and performed a comprehensive histopathological assessment at termination. We further conducted a dose-ranging, 3-month GLP toxicology study in WT Sprague Dawley rats by IT administration. Here, we present all collected preclinical data in rodents to support clinical evaluation of IT-administered AAV9/*MFSD8* as a potential GT for CLN7 patients. This AAV9-based GT strategy can be broadly applied to correct other loss-of-function mutations that lead to CNS disorders. Investigational new drug (IND) application #19766 to initiate a Phase I intrathecal gene transfer trial for AAV9/*MFSD8* was approved by the FDA in December 2020, and the trial is currently enrolling CLN7 patients at Children's Health in Dallas, TX in collaboration with UTSW Medical Center (clinicaltrials.gov NCT04737460).

Results

AAV2/*MFSD8* vector rescues lysosomal function in primary fibroblasts from CLN7 patient

To determine whether AAV-mediated expression of WT *MFSD8* could rescue the function of the lysosomal system in fibroblasts from CLN7 patient, we created a self-complementary (sc)AAV2/*MFSD8* vector, which is packaged with an expression cassette comprising a mutant AAV2 inverted terminal repeat (ITR) with the D element deleted (Δ ITR), the low expressing JeT promoter (30, 39), the human *MFSD8* codon-optimized coding sequence (*hMFSD8opt*), simian virus 40 polyadenylation (SV40pA) signal, and WT AAV2 ITR (Figure 1A).

Peripheral tissue biopsies taken from human CLN7 patient show accumulation of storage material typical of the disease in the lysosomal compartments, indicating a compromised function (19, 21). There is also elevated expression of lysosomal cathepsins such as *CTSB* in the CLN7 storage phenotype (6). Since the precise function of CLN7 in the lysosome is not known, a functional lysosomal assay (40, 41) that measures lysosomal beta-glucocerebrosidase (GCase) was used as a surrogate to measure lysosomal function in patient fibroblast cell cultures. Consistent with our previous report (42), there was a significant reduction in lysosomal GCase activity compared to that of a healthy age-matched individual (Figure 1B), suggesting that CLN7 deficiency compromises general lysosomal function.

As an initial proof-of-concept for human *MFSD8* GT, AAV2/*MFSD8* efficacy at improving lysosomal function in cultured fibroblasts from a CLN7 patient was tested. These assays used an AAV2 vector to deliver the *MFSD8* expression cassette to assess the function of the *hMFSD8opt* transgene expression as these cells are not readily transduced by AAV9. An AAV2 vector carrying the gigaxonin (*GAN*) transgene driven by the JeT promoter was used as a negative control. In addition to the JeT promoter, a stronger UsP promoter was used to test for a potential additional benefit from higher *MFSD8* transgene expression. Note that the JeT and UsP promoters are identical, except UsP contains an intron that boosts expression. The AAV2/JeT-*MFSD8* titers tested were 1×10^3, 1×10^4, 1×10^5, and 5×10^5 vector genomes (vg)/cell. The AAV2/JeT-*GAN* and the AAV2/UsP-*MFSD8* titers used were 1×10^5 vg/cell.

The enzymatic activity in the fibroblasts transduced with AAV2/JeT-*GAN* was considered the baseline to which activity in test cohorts was compared. There was a dose-dependent increase in the lysosomal function with AAV2/JeT-*MFSD8* titers of 1×10^4 and 1×10^5 vg/cell (Figure 1C-D). There was about a 2-fold increase in lysosomal and total GCase activity at the 1×10^5 vg/cell multiplicity of infection (MOI). At the highest MOI of 5×10^5 vg/cell, there was no significant improvement in lysosomal GCase activity (Figure 1C-D). Although toxicity from increased *hMFSD8opt* expression or high AAV doses are a possibility, a general cell staining assay that measures total cell volume did not demonstrate any significant changes compared to other conditions tested (Supplemental Figure 1A-B). The fold change in enzymatic activity with the JeT promoter-driven *MFSD8* at the 1×10^5 vg/cell MOI and the stronger UsP promoter at the 1×10^5

vg/cell MOI was similar (Figure 1C-D), suggesting that there is no additional benefit to rescuing lysosomal function by using the stronger promoter at this dose. Similar patterns were seen in total and lysosomal *CTSB* activity (Supplemental Figure 1E-F).

Further evaluations were performed at a fixed titer of 1×10^5 vg/cell to compare the JeT promoter and UsP promoter, in terms of their relative abilities to drive expression of *MFSD8* mRNA and protein, as well as to confirm the lysosome rescue results. While both promoters drove similar levels of *MFSD8* mRNA expression, the UsP promoter drove more MFSD8 protein expression compared to JeT promoter, suggesting that there is a saturating level of transcript/protein above which additional rescue is not achieved (Figure 1E-F and Supplemental Figure 1G). In terms of rescuing lysosomal function, the data from 2 additional independent experiments showed increased GCase enzymatic activity with AAV2/JeT-*MFSD8* treatment relative to AAV2/JeT-*GAN* (Supplemental Figure 1C-D). However, as originally assessed, the 1×10^5 vg/cell dose with a stronger UsP promoter did not result in a significant increase in total and lysosomal GCase activity above that seen with JeT promoter at the same titer (Supplemental Figure 1C-D). Taken together, the data from Figure 1 and Supplemental Figure 1 indicate JeT-driven *MFSD8* expression at the vector dose of 1×10^5 vg/cell rescues the lysosomal function in fibroblasts from a CLN7 patient, and there is no observed additional benefit to overexpressing *MFSD8* with a stronger promoter.

AAV9/*MFSD8* GT in KO mice rescues GCase activity, induces *MFSD8* mRNA expression, and confers trends of decreased SCMAS accumulation and GFAP immunoreactivity

To test whether the AAV9/*MFSD8* vector rescues the phenotypes in *Mfsd8*$^{-/-}$ (KO) mice, balanced groups of male and female KO mice were injected IT at postnatal day (p)7-10 (pre-symptomatic cohorts) or p120 (early-symptomatic cohorts) with a single high (5×10^{11} vg/mouse) or low (1.25×10^{11} vg/mouse) dose of AAV9/*MFSD8* vector (Figure 2A). At 4.5 months old, 3 males and 3 females from each dose or control group treated at p7-10 were taken down to evaluate GCase activity (Figure 2B), vector biodistribution (Figure 2C), *MFSD8* mRNA expression (Figure 3), and early histological signs (Figure 4-5 and Supplemental Figure 2-3) of treatment efficacy. Compared to WT or Het control mice, there was significantly reduced GCase activity in brain lysates of KO mice receiving vehicle treatment (KO-Veh), which was fully rescued by the low (KO-Low) or high (KO-High) dose of AAV9/*MFSD8* vector (Figure 2B). IT delivery of AAV9/*MFSD8* vector resulted in a dose-dependent increase of *MFSD8* vector DNA across the CNS (brain and spinal cord) and peripheral organs (heart, lung, liver, kidney, spleen, gonad, and triceps). The *MFSD8* vector DNA is concentrated closest to the injection site in the spinal cord and detected at lower levels in multiple brain regions. In the peripheral organs, similar high amounts of *MFSD8* DNA persist in heart, lung, and liver and to the less extent in kidney, spleen, gonad, and triceps (Figure 2C). Animals receiving either the low or high dose of AAV9/*MFSD8* vector had detectable levels of transgene *hMFSD8*opt mRNA in all tissues and brain regions assessed (Figure 3). The high dose group had significantly higher mRNA levels than the KO-Veh group.

In CLN7 disease, there is progressive neurodegeneration accompanied by neuroinflammation evidenced by astrocytosis and microgliosis (43). Histopathology of CLN7 tissue shows similar changes in the brain tissue of patients (4) and in mouse models (6). Immunohistochemistry (IHC) with GFAP and Ionized calcium binding adaptor molecule 1 (Iba1) antibodies identify pronounced astrogliosis and microgliosis respectively in CLN7 deficient mice (6). SCMAS and sphingolipid activator proteins (Saposins A and D) are components of the autofluorescent storage material retained in the lysosomes of neuronal tissue in LSDs (5, 6, 24).

IHC with primary antibody against SCMAS was used to assay the accumulation in neuronal tissue isolated from the mice at the age of 4.5 months old. The increase in SCMAS can be observed as higher amounts of brown stain in these tissue sections (Figure 4A). Accumulation of SCMAS was evident in KO-Veh animals compared to Het controls in the cortex, hippocampus, and spinal cord, but not in the cerebellum (Figure 4B). The low dose of AAV9/*MFSD8* had minimal effect on SCMAS staining in these same tissue regions. It should be noted that in the cerebellum and hippocampus, variable and sometimes high background staining made the automated image analysis inconsistent at times, which may explain the apparent increase of SCMAS upon low dose treatment in the cerebellum. Qualitatively and without blinding, our opinion is that there is not an increase in SCMAS staining in the cerebellum. In contrast, the high dose of AAV9/*MFSD8* showed trends of reduced SCMAS accumulation by up to 50.2% in the brain and spinal cord of KO mice, although the differences compared to vehicle-injected KO mice were not statistically significant (Figure 4B and Supplemental Table 1).

GFAP immunoreactivity was significantly increased in the cortex of KO-Veh group mice compared to Het controls at the age of 4.5 months old and the high dose of AAV9/*MFSD8* tended to reduce GFAP immunoreactivity by 38.8% in the cortex of KO mice (Figure 5 and Supplemental Table 1). Similar trends of increased GFAP immunoreactivity were observed in the hippocampus, cerebellum, and spinal cord of KO-Veh group, which showed consistent trends of reduction upon treatment with AAV9/*MFSD8*, but none of the differences were statistically significant (Figure 5 and Supplemental Table 1).

Cluster of differentiation 68 (CD68) immunoreactivity is an alternative maker than Iba1 for microglia, but this was not significantly increased in any brain region analyzed in any group compared to KO-Veh at the age of 4.5 months old (Supplemental Figure 2 and Supplemental Table 1). $NeuN^+$, total cell numbers and the $NeuN^+$/Total cell ratio were not significantly changed in any brain region analyzed in any group compared to KO-Veh at the age of 4.5 months old (Supplemental Figure 3 and Supplemental Table 1). Taken together, these data suggest that the AAV9/*MFSD8* GT is effective at slowing or preventing histological signs of disease progression, but that these effects are dose dependent and require a high dose to be effective.

AAV9/*MFSD8* GT improves survival rate, extends median lifespan, and maintains normal body weight longer in KO mice

There is increased mortality in the KO mice along with associated behavioral deficits (6). We found that KO-Veh animals started experiencing mortality after 2 months of age, and survival drastically decreased between 6 and 11 months old (Figure 6A). AAV9/*MFSD8* administration had a significant effect on survival in both an age-dependent and dose-dependent manner, with the early treatment and high-dose group showing a larger increase survival, whereas the late treatment and low-dose groups showed moderately increased survival (Figure 6A). The IT high dose of AAV9/*MFSD8* at p7-10 resulted in a greater than doubling of median lifespan (16.8 months vs 7.8 months in KO-Veh mice) (Figure 6A). There was no survival benefit when KO mice were treated at 6 months old with the high IT dose (Supplemental Figure 4), further supporting that CLN7 needs to be treated early to be effective. There was a notable drop in body weight as KO mice approached median survival age across all dose cohorts (Figure 6B-E). All KO-Veh mice lost body weight rapidly from approximately 6 months old, whereas AAV9/*MFSD8* treated KO mice showed an age- and dose-dependent maintenance of normal body weight for a longer time. No neurologic symptoms or general malaise related to the treatment was observed. These results suggest that AAV9/*MFSD8* GT is effective and safe in this preclinical disease model.

AAV9/*MFSD8* GT restores impaired behavioral phenotypes in KO mice

There are motor deficits including hindlimb paralysis, tremors, and epilepsies in the KO mice (6) that correlate with the neurodegenerative manifestation in CLN7 patient populations (23, 24). To test if AAV9/*MFSD8* GT ameliorates these deficits, mouse cohorts underwent a batter of behavioral testing which included Rotarod, Open Field, Marble Burying, and Wire Hang tests (Figure 7). These tests were selected based on known or suspected deficits in the KO mouse model, as well as for their ability to be repeated longitudinally. Performance of mice on the Rotarod reflects motor coordination capabilities (44). The cohorts were tested for their ability to walk forward without falling on a horizontal rod rotating on its long axis at an accelerating speed. Latency to fall is recorded over multiple trials per mouse. This assay quantifies loss or improvements in the motor coordination differences between untreated and treated KO mice. The Open Field test in mice is a tool to assess novel environment exploration, anxiety-related behavior, and general locomotor activity (45). Performance of the KO mice on these tests had not been previously reported, thus this testing will serve to assess both the utility of Open Field test for CLN7-specific phenotype and for potential therapeutic rescue. Additionally, mice were tested for Marble Burying, a behavioral assay which utilizes the natural digging behavior of mice. Increased digging/ marble burying can be observed in multiple models of psychiatric disease (46). Wire Hang was also used to test grip strength.

No or minimal behavioral deficits were observed between Het control animals and KO-Veh or KO-AAV9/*MFSD8* dosed animals at 2 or 4 months of age (Figure 7). At 6 months old, significant behavioral deficits were observed in the KO-Veh group compared to Het controls in multiple assays including Rotarod, Open Field, and Marble Burying, with deficit rescue observable in the p7-10 high dose group. KO-Veh animals performed poorly on the Rotarod compared to Het controls, with a significantly shortened latency to fall across 8 trials (Figure 7A). This deficit was

ameliorated in the p7-10 high dose group, which performed significantly better than the KO-Veh group and was not significantly different from the Het control group. In the Open Field, KO-Veh animals were hyperactive, traveling a greater total distance during the testing period, and spent significantly more time on the periphery of the testing arena compared to Het controls (Figure 4B-D). Spending more time in the periphery of the testing arena in KO-Veh animals is indicative of anxiety-like behavior and was normalized in the p7-10 high dose group. In Marble Burying, KO-Veh mice buried significantly fewer marbles than Het controls, as did both KO low-dose groups (Figure 4E). This was an unexpected finding, since mouse models of anxiety and psychiatric disorders show an increase in digging/ marble burying; however, studies have also shown that hippocampal lesions can reduce these natural behaviors (47). While there was a trend toward normalization of marble-burying behavior in the high dose treatment groups, it was not statistically significant. There were no significant differences between any groups in Wire Hang performance (Figure 7F) at 6 months old.

Only 6 KO-Veh animals survived to the 9-month testing, and these animals were unable to stay on the Rotarod testing apparatus for more than a few seconds (Figure 7A). All treated animals performed better on the Rotarod than KO-Veh animals, with early treatment achieving better benefits. In the Open Field, there were only significant differences in the total distance traveled (Figure 7B-D). The p7-10 and p120 high dose treated animals remained hyperactive compared to Het controls and KO-Veh animals.

All KO-Veh animals died by 12 months of age and only one p120 low dose animal survived to the 12-month testing (Figure 6A). Thus, the behavior tests were mainly performed on other groups including Het controls, p7-10 low dose, p7-10 high dose, and p120 high dose (Figure 7A-D). The majority of treated animals were able to perform on the Rotarod, with only the p7-10 high dose group having a comparable latency to fall with the Het controls (Figure 7A). In the Open Field, the p7-10 treated animals remained hyperactive (Figure 7B).

There were only a few treated KO animals alive by 15 months of age and no animals alive by 18 months of age in other treatment groups. Remaining animals were either Het controls or KOs treated with p7-10 high dose (Figure 6A). The remaining KO animals treated with p7-10 high dose were still able to perform well on the Rotarod and Open Field comparable to Het controls (Figure 7A-D).

Taken together, there were significant behavioral deficits starting from 6 months old in the KO mice and some deficits seen on the Rotarod and Open Field were completely restored in the p7-10 high dose group, with a trend towards improvement in some other treatment groups. All these results indicate positive treatment effects of AAV9/*MFSD8* GT in both survival and quality of life.

AAV9/*MFSD8* GT is safe and well tolerated in WT mice in a non-GLP study

To demonstrate the long-term safety of the AAV9/*MFSD8* vector, WT C57BL/6J mice were injected IT with the AAV9/*MFSD8* vector in a non-GLP study (Figure 8A). The mice were

randomized to different groups, injected IT with 5 µL of vehicle or different doses of AAV9/*MFSD8* vectors from UNC (University of North Carolina - Vector Core) or Vigene (Vigene Biosciences, Inc.), and monitored up to one year following injection for body weight (BW), survival, adverse events, and histopathology evaluation. The UNC- and Vigene- produced vectors were re-titered in parallel, then evaluated for equivalency by conducting a limited biodistribution analysis after intravenous injection in mice at the same dose. Biodistribution results demonstrated that they were functionally equivalent (Figure 8B). In this non-GLP study, there was no significant difference in BW between groups within male or female mice at any point of assessment and any dose tested (Figure 8C-D). There were no obvious signs of morbidity in the adult WT mice dosed with AAV9/*MFSD8* at doses up to 9.50×10^{11} vg/mouse over the duration of the study. There were four unexpected deaths in this study: one animal found dead in the control group injected with vehicle with no obvious reason, one found dead in the treated group injected with 4.47×10^{11} vg/mouse with no obvious reason, one found dead in the treated group injected with 9.50×10^{11} vg/mouse which was most likely caused by overgrooming-induced severe back injury, and one euthanized for animal welfare in the treated group injected with 9.50×10^{11} vg/mouse because of overgrooming-induced severe back and leg injury. Therefore, there was no significant difference of survival rates between groups within male or female mice (Figure 8E-F). At the end of the experiment, the tissues of the 46 surviving mice were sent out for a blinded histopathology evaluation, where it concluded that none of the microscopic findings are suggestive of adverse effects related to vector administration in these mice (Supplemental report from Dr. Wight-Carter). Taken together, all these results demonstrate that doses up to 9.50×10^{11} vg/mouse are well tolerated in WT C57BL/6J mice up to 12 months following the treatment.

AAV9/*MFSD8* GT is safe and well tolerated in WT rats in a GLP study

To further demonstrate the safety and biodistribution pattern of AAV9/*MFSD8* vector, WT CD [Crl:CD(SD)] rats were injected with AAV9/*MFSD8* vector in a GLP study (Figure 9A). The animal study was performed by Charles River Laboratories, Inc. (Mattawan MI). Male and female CD rats were randomized into cohorts, with 5 males and 5 females per cohort, and dosed by a qualified laboratory technician. At the initiation of dosing, the animals assigned to the study were approximately 56 to 63 days old and injected IT once in each animal with a dose of 5×10^{11}, 2×10^{12}, or 6×10^{12} vg/rat. All animals were monitored up to 90 days following the injection for BW, survival, biodistribution, Rotarod performance, and toxicology including blood chemistry and histopathology. Rats were sacrificed on day 7, 28, or 90 post injection, and tissues were collected for biodistribution and toxicity evaluation. In this GLP rat study, there was no significant difference in BW between groups within male or female rats at any point of assessment and any dose tested (Figure 9B). There were no obvious signs of morbidity or mortality in the adult WT rats dosed with AAV9/*MFSD8* at doses up to 6×10^{12} vg/rat over the duration of the study. Total genomic DNA was purified from tissue samples collected at necropsy day 28, using a Qiagen Qiacube HT. qPCR was used to determine the quantity of the *MFSD8* transgene per diploid rat genome (Figure 9C). Consistent with the results in mice (Figure 2C), IT delivery of AAV9/*MFSD8*

vector resulted in a dose-dependent increase of *MFSD8* vector DNA across the CNS (brain and spinal cord) and peripheral organs (heart, lung, liver, kidney, ovary, and testes). The *MFSD8* vector DNA is concentrated closest to the injection site in the spinal cord and detected at lower levels in multiple brain regions. In the peripheral organs, similar high amounts of *MFSD8* DNA persist in liver and heart and to the less extent in testes, ovary, lung, and kidney. The pattern of CLN7 biodistribution in this study is consistent with that expected from AAV9 and observed in a previous study from Dr. Gray's laboratory where a similar vector, scAAV9/JeT-*hGANopt*-SpA, was injected IT to WT rats at a dose of 6.6×10^{11} vg/rat (Gray lab, unpublished findings). Collectively, IT delivery of AAV9/*MFSD8* resulted in broad *MFSD8* biodistribution across the rat body, which is considered to portray the normal biodistribution pattern expected for an AAV9 vector in rats with vector biodistribution increasing linearly with dose. Moreover, there was no indication of reduced vector biodistribution compared to that expected, suggesting a lack of vector loss due to cellular toxicity. Clinical pathology revealed a minor immune or inflammatory stimulus including increases in lymphocyte and leukocyte count, increases in fibrinogen and globulin concentration, and decreases in triglyceride concentration (Supplemental Table 2), which lacked definitive microscopic correlates and were mostly resolved by the end of the observation period. All animals survived to their scheduled terminal necropsies. At the end of the experiment, the tissues of all enrolled rats were sent out for blinded comprehensive histopathology evaluation, which concluded that there were no scAAV9/*MFSD8* related macroscopic findings or microscopic changes directly attributable to the administration of test article, except significantly increased thymus weights in males at the high dose. Microscopically, only minimal and multifocal hemorrhages were seen in the thymus. The increased thymus weights had no clear histopathological correlation and therefore were considered to have unclear toxicological significance (Supplemental report from CRL). Taken together, administration of the scAAV9/*MFSD8* vector up to 6×10^{12} vg/rat resulted in dose-dependent increase of *MFSD8* vector DNA across the rat body and was not associated with any mortality, clinical observations, altered Rotarod performance, body weight, or food consumption changes, further demonstrating the safety of the AAV9/*MFSD8* vector.

Discussion

Recombinant AAV9-mediated GT has been extensively used in preclinical and clinical studies for the treatment of CNS disorders. Efficacy with AAV9 has been demonstrated in numerous preclinical models of CNS disorders and in some clinical studies using an IT route of administration. In addition, efficacy with AAV9 has also been demonstrated in multiple Batten diseases including CLN3, CLN6, and CLN8 using other routes of administration (48-50). Here we tested the feasibility and efficacy of an AAV9-based strategy to deliver the codon-optimized human *MFSD8* gene in fibroblasts from CLN7 patient in vitro as well as in a CLN7 mouse model, to investigate whether this would predict a benefit to pediatric patients with CLN7 disease.

Preclinical in vivo studies were initiated in Dr. Gray's laboratory at the UNC Gene Therapy Center and completed at UTSW Medical Center. IT administration of AAV9/*MFSD8* in KO mice, a severe mouse model of the human disease, conferred a consistent but non-significant trend of decreased accumulation of SCMAS and astrogliosis, major hallmarks of the underlying disease pathology. There were no findings of behavioral deficits at 2 or 4 months of age in KO-Veh animals compared to Het controls, however there were significant behavioral deficits at 6 months of age. This is consistent with previously published data on this mouse model, where behavioral deficits were seen starting at 6 months of age (5, 6). Some deficits in Rotarod and Open Field were completely restored in the p7-10 high dose group, with a trend towards improvement in some other treatment groups (i.e., lower dose or later age of treatment). The extended lifespan in all treatment groups demonstrates that AAV9/*MFSD8* treatment can be effective at extending life in this animal model of Batten disease. Further, surviving treated animals can still perform similarly to Het controls on a Rotarod beyond 9 months of age, suggesting that treatment can protect quality of life in addition to extending survival. Considering both the age- and dose-dependent increase in survival, along with the behavioral phenotypic rescue especially in the p7-10 high dose group, it is evident that a high dose at an earlier age provides the largest benefit for survival and quality of life. Previous preclinical studies of CLN6 and CLN8 diseases utilized an intracerebroventricular (ICV) route of administration in newborn mice (48, 49). Our preclinical studies have proved the concept of IT AAV9/*MFSD8* gene replacement as a viable treatment strategy for the treatment of CLN7 disease, administered at later postnatal ages that better model intervention ages relevant to human treatment.

Studies in mice and non-human primates (NHP) using an AAV9 vector carrying the reporter gene green fluorescent protein (GFP) have demonstrated that widespread distribution of the transgene across the spinal cord, dorsal root ganglia (DRG), and brain are achievable after a single IT injection of the vector (34, 51). Compared to an IV route of administration, the IT route favorably directs a greater percentage of vector biodistribution to the CNS (34-38, 51-53). Notably, AAV9 does distribute to peripheral organs following an IT injection, but to a considerably lesser extent compared to an IV route. The IT approach is scalable to humans, avoids anti-AAV9 neutralizing antibodies in the blood, and reduces the risk of transgene overexpression in peripheral organs. Biodistribution of AAV9/*MFSD8* in rats and qualitative mRNA expression analysis in KO mouse models following IT AAV9/*MFSD8* administration suggest the distribution and expression of transgene is comparable to what has been observed with other past IT studies, including those with AAV9/*GAN* which used the same JeT promoter (30). A limitation of our approach is that we would not expect meaningful biodistribution of the AAV9 vector to photoreceptors in the eye by the IT route. Although we did not investigate the potential for vision rescue, we would not expect this treatment approach to prevent photoreceptor degeneration and eventual vision loss. As we did not directly compare the IT route to an IV administration in this study, we cannot speculate whether additional biodistribution to peripheral organs could have led to additional treatment benefits. Combining the IT dose with an ocular gene therapy, a combined IV administration, optimized vector administration approaches, and/or an improved capsid all represent avenues to increase

treatment efficacy. Conversely, we must consider that the lack of complete rescue of the mouse model at the high dose and early intervention we used may indicate the edge of AAV9's ability to fully rescue a disorder when delivering a gene that acts in a cell-autonomous manner, unless further steps are taken to improve the gene transfer technology.

The non-GLP toxicology studies were conducted on juvenile WT mice, showing that the AAV9/*MFSD8* vector does not affect BW or body condition over a 1-year period of longitudinal monitoring. Further, a comprehensive blinded histopathology assessment did not find any evidence of toxicity due to AAV9/*MFSD8* at 1-year post-injection. Collectively, IT AAV9/*MFSD8* doses up to 9.50×10^{11} vg/mouse were deemed safe and well tolerated in WT mice. There were no toxicities observed in either the in-life portion of the study or after microscopic examination of major tissues. If scaled to humans by cerebrospinal fluid (CSF) volume (assuming 35 uL CSF volume in mice and 140 mL CSF volume in humans), the mouse dose of 9.5×10^{11} vg in 5 uL would translate to a human dose of 3.8×10^{15} vg in a volume of 20 mL. This highest dose injected in the mice is a 3.8-fold higher titer than the highest dose proposed for humans ($1x10^{15}$ total vg), in twice the volume proposed for humans (https://clinicaltrials.gov/ct2/show/NCT04737460). Thus, the maximum tolerated dose in mice up to one-year post-injection provides a further safety margin above what is proposed in humans.

The pivotal GLP toxicology study was conducted in normal juvenile rats by Charles River laboratories. This GLP rat toxicology study found no significant test article-related effects on study parameters, with the exception of increased thymus weights in males at the high dose, suggesting AAV9/*MFSD8* was overall well-tolerated with the IT doses up to 6×10^{12} vg/rat in WT rats. If scaled to humans by CSF volume (assuming 250 uL CSF volume in rat and 140 mL CSF volume in humans), the rat dose of 6×10^{12} vg in 60 uL would translate to a human dose of 3.4×10^{15} vg in a volume of 33.6 mL. This highest dose injected in the rats is a 3.4-fold higher titer than the highest dose proposed in humans, in over 3 times the volume proposed in humans. Thus, the maximum tolerated dose in rats up to three months post-injection provides a further safety margin above what is proposed in humans. Based on the mouse and rat studies combined, we report a no-observed-adverse-effect-level (NOAEL) for IT AAV9/*MFSD8* as 3.8×10^{15} vg (scaled human dose), although it could be higher considering that higher doses were not tested.

An identified risk of inflammatory damage to DRG is an emerging safety concern of CNS-directed AAV GT, which has been reported from recent non-clinical studies in NHPs as well as piglets (54-56). In a study assessing IT administration of AAV across over 200 NHPs assessed in one center, minimal to mild DRG histopathology was a consistent finding across most animals, independent of the transgene (55). However, that same study noted minimal correlations to any adverse behavioral symptoms, or physiological biomarkers such as altered nerve conduction. In a follow-up report, incorporation of a miRNA binding site specific to DRG resolved this histopathology, suggesting that high transgene expression was driving the toxicity in DRG (56). Considering this putative link between transgene overexpression and DRG toxicity, there is value in our initial in vitro experiment comparing promoters, in which we concluded that the minimal synthetic JeT

promoter was sufficient to rescue cellular phenotypes with no additional value in overexpressing *MFSD8* (Figure 1). We performed a long-term safety study in mice and a short-term safety study in rats, however a notable limitation of rodent models is that they have not been demonstrated to model the DRG toxicity that has been observed in pigs and NHPs. However, our group has observed DRG histopathology in rats following IT administration of an unrelated AAV9 vector and transgene in another GLP safety study, suggesting that rats may be capable of modeling this DRG histopathology (data not shown). Nonetheless, after careful examination there was no sign of DRG toxicity in the mouse and rat safety studies for AAV9/*MFSD8*.

In conclusion, the results achieved in these studies demonstrate that AAV9/*MFSD8* is both effective and well tolerated in preclinical models, providing strong proof-of-concept evidence that AAV9/*MFSD8* GT should be considered for human translation. Since the CSF volume of humans is relatively static after 3 years old (57) whereas CNS cells degenerate as CLN7 disease deteriorates, we suggest a final target dose of 1×10^{15} vg total vg in 10 mL in CLN7 patients > 3 years old. Higher doses could be considered and may be justified from our preclinical data, if the vector could be concentrated above 1×10^{14} vg/mL or if a higher injection volume could be utilized. Our data also emphasizes the value of intervening as early in the disease course as possible to maximize treatment benefit. If patients $\leqslant$ 3 years old were treated, it might be appropriate to scale doses lower to account for reduced brain and CSF volume. It is worth noting that while CLN7 is a lysosomal storage disease, MFSD8 is a membrane-bound protein, and this disease is not thought to benefit from cross-correction. Thus, the conclusions from this study may translate to other AAV9-based gene replacement strategies for related neurological disorders involving genes with cell-autonomous effects. IND #19766 to initiate a Phase I intrathecal gene transfer trial for AAV9/*MFSD8* was approved by FDA in December 2020, and the trial is enrolling CLN7 patients at Children's Health in Dallas, TX in collaboration with UTSW Medical Center (clinicaltrials.gov identifier NCT04737460).

Materials and Methods

Plasmid design and development

We designed and developed the JeT-*hMFSD8opt*-SV40pA plasmid (Figure 1A) containing the transgene of a human *MFSD8* codon-optimized construct (*hMFSD8opt*). The transgene consists of a human *MFSD8* codon-optimized DNA coding sequence of 1557 bp between a 164 bp JeT promoter (30, 39) and a 123 bp SV40pA polyadenylation signal. The JeT promoter and SV40pA are utilized for their small sizes allowing for packaging into an scAAV vector, as well as to mediate the minimal amount of expression needed.

scAAV2/MFSD8 and scAAV9/MFSD8 vector preparation

The established plasmid was packaged into scAAV2 and scAAV9 vectors (58) which are 10-100 times more efficient at transduction compared to traditional single-stranded (ss)AAV vectors (59, 60). The scAAV2 vector was produced at the UNC Vector Core. For scAAV9 vector, three lots of vectors were produced by either the UNC Vector Core or Vigene Biosciences, Inc. Both research grade vectors by two vendors showed equivalent in vivo biodistribution patterns, indicating similar biopotency (Figure 8B). Vigene also produced a toxicology lot of AAV9/*MFSD8* which was used in the cohorts of KO mice to assess efficacy of the GT and in WT rats to assess safety of the GT in the GLP toxicology study. The AAV2 vectors and the research-grade AAV9 vector made at UNC were titered by qPCR and confirmed by silver stain (61). The vectors produced at Vigene underwent quality control release testing. The quality control summaries of the scAAV9/*MFSD8* vectors are included in the Supplemental information.

In vitro CLN7 patient fibroblast culture and treatment

An assay to measure lysosomal function in patient fibroblasts was developed by the Mazzulli lab (40, 41). The fibroblasts were obtained from peripheral tissue biopsies of a human CLN7 patient with compound mutations of c.1102G→C (p.Asp368His) and i6SVA insertion (42), treated with the AAV2 vectors at the indicated MOIs for 5 days, and loaded with cascade blue dextran at 1 mg/mL (D-1976, Life Technologies) for 1 day before the measurement of enzyme activity. All enzymatic assays were performed with n=4-6 separate culture wells and in 2-3 different passages of fibroblasts. The slight difference in "n" number between total and lysosomal activity is due to occasional cell attachment/clumping issues on the bafA1 treated side leading to exclusion of those samples.

Mfsd8$^{-/-}$ (KO) mice

Two different KO mouse models (tm1a and tm1d alleles) were generated and characterized by Dr. Storch's laboratory in Germany (5, 6). The phenotype of the tm1a allele is much milder than the typical human disease, while the phenotype of the tm1d allele is comparable to the human CLN7 clinical presentation. Therefore, the tm1d allele mouse model was used in our preclinical studies. The tm1d KO mice were generated by targeted deletion of exon 2 in *Mfsd8* gene, which recapitulates key features of human CLN7 disease (6). Tm1d KO mice were identified by toe tattooing at p7-10 and then randomized into treatment groups based on the ID numbers assigned to them at genotyping.

Efficacy study plan in KO mice

The experimental design for the in vivo efficacy study is summarized in Figure 2A. In brief, balanced groups of male and female KO mice were injected IT at p7-10 (pre-symptomatic cohorts) or p120 (early-symptomatic cohorts). For IT, 5 µL of high (5×10^{11} vg/mouse) or low (1.25×10^{11} vg/mouse) dose of scAAV9/*MFSD8* vector was administrated via lumber puncture. All mice were weighed weekly up to 4 weeks old and monthly thereafter, as well as observed for overt signs of adverse effects at the times of weighing. The survival rate was calculated, and cause of mortality

was investigated by a veterinary staff whenever possible. Behavioral testing was performed blindly on all study cohorts at 2, 4, 6, 9, 12, 15, and 18 months old. At 4.5 months old, 3 males and 3 females from each cohort treated at p7-10 were sacrificed to evaluate GCase activity, vector biodistribution, *MFSD8* mRNA expression by RNAscope, and early histological signs of treatment efficacy by IHC. All remaining mice were maintained to evaluate long-term survival, behavioral phenotypes, and safety until they required humane euthanasia or reached 24 months old, the planned endpoint of the experiment.

Tissue preparation for GCase activity, vector biodistribution, RNAscope, and IHC staining

At necropsy, animals were deeply anesthetized via an intraperitoneal injection of a 2.5% avertin solution in normal saline. Animals were perfused for 5 min with 1×PBS containing 1 U/mL heparin. The right half of tissues were harvested for GCase activity in brain lysates (40, 41) and vector biodistribution in all tissues collected (62). The left half of tissues were harvested and fixed in 10% neutral-buffered formalin (NBF) for 24 h and transferred to 70% ethanol. Tissues were then processed, embedded in paraffin, and cut into 5 µm sections. Separate sections were used for RNAscope to detect *MFSD8* mRNA or IHC to stain for SCMAS, GFAP (63), CD68, and NeuN.

Image Analysis

All stained slides with one section for each animal were digitized with a ScanScope slide scanner (Aperio Technologies). Scanned slides were viewed with the ImageScope software package (Version 10.0, Aperio Technologies) and analyzed using custom analysis settings in HALO™ Image Analysis Platform (Halo2.2, Indica Labs). A region of interest (ROI) was hand drawn on each image to allow for analysis by tissue region. Within the brain, regions were drawn around the whole brain, cortex, hippocampus, cerebellum, sub-cortex, and brain stem. For spinal cord samples, the entire tissue area was analyzed. A threshold for each stain was set using positive and negative control images, and the same analysis settings were applied for every image of the same stain. Percent area staining for each marker of interest was recorded for each tissue/ROI. Fiji Image J software was used to count $NeuN^+$ cells and hematoxylin-stained nuclei. Total cells ($NeuN^+$ cells + hematoxylin-stained nuclei) and $NeuN^+$/Total cells ratio were calculated. Analysis was done with the observer blinded to treatment group of each sample.

Behavioral tests

Animals were assessed in a battery of behavioral tests repeated at 2, 4, 6, 9, 12, 15, and 18 months old. Rotarod and Open Field tests were tested at 2-18 months old, while Marble Burying and Wire Hang tests were tested at 2-6 months old. All behavioral tests were conducted by personnel blind to the genotype and treatment of the mice.

Non-GLP safety study in WT BL/6J mice

The non-GLP studies presented in Figure 8A were designed to identify any long-term safety issues of the experimental therapy. The mice were randomized to different groups and injected IT with 5 µL of vehicle or different doses of AAV9/*MFSD8* vectors. Two lots of research-grade AAV9/*MFSD8* vectors were made by the UNC Vector Core or Vigene, and both were used in parallel safety studies. Mice were monitored following the treatment and appropriate supportive or therapeutic interventions were offered. A detailed necropsy was performed to investigate the reason for the ailment. Terminal tissue samples including brain, heart, liver, lung, gonad, spleen, kidney, eyeball, sciatic nerve, cervical spinal cord, and lumbar spinal cord at 12 months following the treatment were collected for histopathological assessment. The final histopathological evaluation on collected tissue samples was performed and reported by Dr. Mary Wight-Carter, DVM, DACVP, Veterinary Pathologist at the Animal Research Center, UTSW Medical Center (Supplemental information).

Safety study in WT CD rats in a GLP study

This animal study was performed by Charles River Laboratories, Inc. (Mattawan, MI). Male and female CD rats were randomized into cohorts, with 5 males and 5 females per cohort, and dosed as shown in Figure 9A. At the initiation of dosing, the animals assigned to study were approximately 56 to 63 days old and weighed between 165 g and 328 g. AAV9/*MFSD8* vector was injected IT once in each animal by a qualified laboratory technician, in a volume of 20 or 60 µL, and a final dose of 5×10^{11}, 2×10^{12}, or 6×10^{12} vg/rat. All animals were monitored up to 90 days following the injection. Rats were sacrificed on day 7, 28, or 90 post injection, and tissues were collected for biodistribution and toxicity evaluation. For biodistribution, total genomic DNA was purified from tissue samples collected at necropsy day 28, using a Qiagen Qiacube HT. qPCR was used to determine the quantity of the *MFSD8* transgene per diploid rat genome. Details of this study are provided in CRL's final report, provided as supplemental information.

Statistical Analysis

All quantitative data in this paper were presented as mean ± SEM, analyzed, and graphed using GraphPad Prism Software (v. 9.2.0, GraphPad Software). A ROUT test was used first to remove any outlier. Only two outliers were excluded from calculation based on the ROUT test (Supplemental Table 1). Data were then tested for normal distribution (Shapiro-Wilk normality test) and homogeneity of variance (Brown-Forsythe test). Data sets that passed these two tests were analyzed using the Student's unpaired t-test for two groups comparison or one-way ANOVA for equal or more than three groups comparison with Dunnett's correction for relevant pairwise comparisons. Data sets that did not pass tests for normality or homogeneity of variance were analyzed using the Mann-Whitley test for two groups comparison or Kruskal-Wallis test with Dunn's correction for relevant pairwise comparisons. For survival analysis, data shown in the Kaplan-Meier survival curve were compared with the Log-rank (Mantel-Cox) test. Two-way ANOVA with repeated measures was used for BW analyses. A $p < 0.05$ was considered as significant for all statistical analyses.

For more detailed information, please refer to **Supplemental Materials and Methods.**

Study approval

All researchers working with mice were approved by the Institutional Animal Care and Use Committee (IACUC) of the UNC at Chapel Hill or the UTSW Medical Center. The in life GLP toxicity study was performed at Charles River Laboratory and was approved by their IACUC.

Author contributions

XC and SJG designed the experiments. XC, FS and SJG coordinated studies with collaborators and core facilities and wrote the manuscript. XC, TD, YH, FS, NRB, and JRM performed the experiments. XC, TD and FS analyzed all data and prepared all figures for the manuscript. YH, NRB, and JRM helped preparing the manuscript**.** SJG oversaw all activities related to the project and acquired all funding for the work.

Conflict of interest statement: XC received a consulting fee from Neurogene Inc. SJG received patent royalties for intellectual property (IP) licensed to Asklepios Biophama, but this IP was not used in this study, and he received consulting and royalty income from Neurogene Inc. UT Southwestern Medical Center may benefit from the potential commercialization of the technology described in this manuscript.

Acknowledgments

This study was supported primarily by funding from Mila's Miracle Foundation, with additional funding from the Batten Hope Foundation to S.J.G. We thank Jackson laboratories for providing the initial mouse breeders and UNC and Vigene Biosciences, Inc. for producing the vectors used in these studies. We thank Dr. Shari Birnbaum and her team at the UTSW Phenotypic Core Facility for performing all the behavioral tests. We acknowledge Dr. Mary Wright-Carter and her team at the UTSW Diagnostic Laboratory for their toxicity evaluation and histopathological safety report.

Address correspondence to: Dr. Steven J Gray, Department of Pediatrics, University of Texas Southwestern Medical Center. Room NA2.508, 6000 Harry Hines Blvd., Dallas, TX 75390. Phone: (214) 648-0670; Email: Steven.Gray@UTSouthwestern.edu

References

1. Siintola E, et al. The novel neuronal ceroid lipofuscinosis gene MFSD8 encodes a putative lysosomal transporter. *Am J Hum Genet.* 2007;81(1):136-146.

2. Mole SE, Cotman SL. Genetics of the neuronal ceroid lipofuscinoses (Batten disease). *Biochim Biophys Acta.* 2015;1852(10 Pt B):2237-2241.

3. Pao SS, et al. Major facilitator superfamily. *Microbiol Mol Biol Rev.* 1998;62(1):1-34.

4. Sharifi A, et al. Expression and lysosomal targeting of CLN7, a major facilitator superfamily transporter associated with variant late-infantile neuronal ceroid lipofuscinosis. *Hum Mol Genet.* 2010;19(22):4497-4514.

5. Damme M, et al. Gene disruption of Mfsd8 in mice provides the first animal model for CLN7 disease. *Neurobiol Dis.* 2014;65:12-24.

6. Brandenstein L, et al. Lysosomal dysfunction and impaired autophagy in a novel mouse model deficient for the lysosomal membrane protein Cln7. *Hum Mol Genet.* 2016;25(4):777-791.

7. Bagshaw RD, et al. A proteomic analysis of lysosomal integral membrane proteins reveals the diverse composition of the organelle. *Mol Cell Proteomics.* 2005;4(2):133-143.

8. Schroder B, et al. Integral and associated lysosomal membrane proteins. *Traffic.* 2007;8(12):1676-1686.

9. Guo J, et al. A rare homozygous MFSD8 single-base-pair deletion and frameshift in the whole genome sequence of a Chinese Crested dog with neuronal ceroid lipofuscinosis. *BMC Vet Res.* 2015;10:960.

10. Palmer DN. The relevance of the storage of subunit c of ATP synthase in different forms and models of Batten disease (NCLs). *Biochim Biophys Acta.* 2015;1852(10 Pt B):2287-2291.

11. Aiello C, et al. Mutations in MFSD8/CLN7 are a frequent cause of variant-late infantile neuronal ceroid lipofuscinosis. *Hum Mutat.* 2009;30(3):E530-540.

12. Kousi M, et al. Mutations in CLN7/MFSD8 are a common cause of variant late-infantile neuronal ceroid lipofuscinosis. *Brain.* 2009;132(Pt 3):810-819.

13. Boya P, Kroemer G. Lysosomal membrane permeabilization in cell death. *Oncogene.* 2008;27(50):6434-6451.

14. Repnik U, et al. Lysosomes and lysosomal cathepsins in cell death. *Biochim Biophys Acta.* 2012;1824(1):22-33.

15. Aldahmesh MA, et al. Neuronal ceroid lipofuscinosis caused by MFSD8 mutations: a common theme emerging. *Neurogenetics.* 2009;10(4):307-311.

16. Stogmann E, et al. A novel mutation in the MFSD8 gene in late infantile neuronal ceroid lipofuscinosis. *Neurogenetics.* 2009;10(1):73-77.

17. Kousi M, et al. Update of the mutation spectrum and clinical correlations of over 360 mutations in eight genes that underlie the neuronal ceroid lipofuscinoses. *Hum Mutat.* 2012;33(1):42-63.

18. Santorelli FM, et al. Molecular epidemiology of childhood neuronal ceroid-lipofuscinosis in Italy. *Orphanet J Rare Dis.* 2013;8:19.

19. Mandel H, et al. Clinico-pathological manifestations of variant late infantile neuronal ceroid lipofuscinosis (vLINCL) caused by a novel mutation in MFSD8 gene. *Eur J Med Genet.* 2014;57(11-12):607-612.

20. Patino LC, et al. Exome sequencing is an efficient tool for variant late-infantile neuronal ceroid lipofuscinosis molecular diagnosis. *PloS one.* 2014;9(10):e109576.

21. Craiu D, et al. Rett-like onset in late-infantile neuronal ceroid lipofuscinosis (CLN7) caused by compound heterozygous mutation in the MFSD8 gene and review of the literature data on clinical onset signs. *Eur J Paediatr Neurol.* 2015;19(1):78-86.

22. Di Fruscio G, et al. Lysoplex: An efficient toolkit to detect DNA sequence variations in the autophagy-lysosomal pathway. *Autophagy.* 2015;11(6):928-938.

23. Roosing S, et al. Mutations in MFSD8, encoding a lysosomal membrane protein, are associated with nonsyndromic autosomal recessive macular dystrophy. *Ophthalmology.* 2015;122(1):170-179.

24. Khan KN, et al. Specific Alleles of CLN7/MFSD8, a Protein That Localizes to Photoreceptor Synaptic Terminals, Cause a Spectrum of Nonsyndromic Retinal Dystrophy. *Invest Ophthalmol Vis Sci.* 2017;58(7):2906-2914.

25. Soldati C, et al. Repurposing of tamoxifen ameliorates CLN3 and CLN7 disease phenotype. *EMBO Mol Med.* 2021:e13742.

26. Mole SE, Williams RE. In: Adam MP, et al. eds. *GeneReviews((R))*. Seattle (WA): University of Washington, Seattle 1993.

27. Naldini L. Gene therapy returns to centre stage. *Nature.* 2015;526(7573):351-360.

28. Saraiva J, et al. Gene therapy for the CNS using AAVs: The impact of systemic delivery by AAV9. *J Control Release.* 2016;241:94-109.

29. Choudhury SR, et al. Viral vectors for therapy of neurologic diseases. *Neuropharmacology.* 2017;120:63-80.

30. Bailey RM, et al. Development of Intrathecal AAV9 Gene Therapy for Giant Axonal Neuropathy. *Mol Ther Methods Clin Dev.* 2018;9:160-171.

31. Karumuthil-Melethil S, et al. Intrathecal administration of AAV/GALC vectors in 10-11-day-old twitcher mice improves survival and is enhanced by bone marrow transplant. *J Neurosci Res.* 2016;94(11):1138-1151.

32. Federici T, et al. Robust spinal motor neuron transduction following intrathecal delivery of AAV9 in pigs. *Gene Ther.* 2012;19(8):852-859.

33. Gray SJ, et al. Global CNS gene delivery and evasion of anti-AAV-neutralizing antibodies by intrathecal AAV administration in non-human primates. *Gene Ther.* 2013;20(4):450-459.

34. Snyder BR, et al. Comparison of adeno-associated viral vector serotypes for spinal cord and motor neuron gene delivery. *Hum Gene Ther.* 2011;22(9):1129-1135.

35. Masamizu Y, et al. Local and retrograde gene transfer into primate neuronal pathways via adeno-associated virus serotype 8 and 9. *Neuroscience.* 2011;193:249-258.

36. Bucher T, et al. scAAV9 intracisternal delivery results in efficient gene transfer to the central nervous system of a feline model of motor neuron disease. *Hum Gene Ther.* 2013;24(7):670-682.

37. Haurigot V, et al. Whole body correction of mucopolysaccharidosis IIIA by intracerebrospinal fluid gene therapy. *J Clin Invest.* 2013;123(8):3254-3271.

38. Samaranch L, et al. Strong cortical and spinal cord transduction after AAV7 and AAV9 delivery into the cerebrospinal fluid of nonhuman primates. *Hum Gene Ther.* 2013;24(5):526-532.

39. Tornoe J, et al. Generation of a synthetic mammalian promoter library by modification of sequences spacing transcription factor binding sites. *Gene.* 2002;297(1-2):21-32.

40. Mazzulli JR, et al. alpha-Synuclein-induced lysosomal dysfunction occurs through disruptions in protein trafficking in human midbrain synucleinopathy models. *Proc Natl Acad Sci USA.* 2016;113(7):1931-1936.

41. Valenzano KJ, et al. Identification and characterization of pharmacological chaperones to correct enzyme deficiencies in lysosomal storage disorders. *Assay Drug Dev Technol.* 2011;9(3):213-235.

42. Kim J, et al. Patient-Customized Oligonucleotide Therapy for a Rare Genetic Disease. *N Engl J Med.* 2019;381(17):1644-1652.

43. Cooper JD, et al. Towards a new understanding of NCL pathogenesis. *Biochim Biophys Acta.* 2015;1852(10 Pt B):2256-2261.

44. Deacon RM. Measuring motor coordination in mice. *JoVE.* 2013(75):e2609.

45. Prut L, Belzung C. The open field as a paradigm to measure the effects of drugs on anxiety-like behaviors: a review. *Eur J Pharmacol.* 2003;463(1-3):3-33.

46. Deacon RM. Digging and marble burying in mice: simple methods for in vivo identification of biological impacts. *Nat Protoc.* 2006;1(1):122-124.

47. Deacon RM, Rawlins JN. Hippocampal lesions, species-typical behaviours and anxiety in mice. *Behav Brain Res.* 2005;156(2):241-249.

48. Cain JT, et al. Gene Therapy Corrects Brain and Behavioral Pathologies in CLN6-Batten Disease. *Mol Ther.* 2019;27(10):1836-1847.

49. Johnson TB, et al. AAV9 Gene Therapy Increases Lifespan and Treats Pathological and Behavioral Abnormalities in a Mouse Model of CLN8-Batten Disease. *Mol Ther.* 2021;29(1):162-175.

50. Bosch ME, et al. Self-Complementary AAV9 Gene Delivery Partially Corrects Pathology Associated with Juvenile Neuronal Ceroid Lipofuscinosis (CLN3). *J Neurosci.* 2016;36(37):9669-9682.

51. Gray SJ, et al. Preclinical differences of intravascular AAV9 delivery to neurons and glia: a comparative study of adult mice and nonhuman primates. *Mol Ther.* 2011;19(6):1058-1069.

52. Markakis EA, et al. Comparative transduction efficiency of AAV vector serotypes 1-6 in the substantia nigra and striatum of the primate brain. *Mol Ther.* 2010;18(3):588-593.

53. Samaranch L, et al. Adeno-associated virus serotype 9 transduction in the central nervous system of nonhuman primates. *Hum Gene Ther.* 2012;23(4):382-389.

54. Hinderer C, et al. Severe toxicity in nonhuman primates and piglets following high-dose intravenous administration of an AAV vector expressing human SMN. *Hum Gene Ther.* 2018;29(3):285-298.

55. Hordeaux J, et al. Adeno-Associated Virus-Induced Dorsal Root Ganglion Pathology. *Hum Gene Ther.* 2020;31(15-16):808-818.

56. Hordeaux J, et al. MicroRNA-mediated inhibition of transgene expression reduces dorsal root ganglion toxicity by AAV vectors in primates. *Sci Transl Med.* 2020;12(569):eaba9188.

57. Bleyer WA, Dedrick RL. Clinical pharmacology of intrathecal methotrexate. I. Pharmacokinetics in nontoxic patients after lumbar injection. *Cancer Treat Rep.* 1977;61(4):703-708.

58. Gray SJ, et al. Optimizing promoters for recombinant adeno-associated virus-mediated gene expression in the peripheral and central nervous system using self-complementary vectors. *Hum Gene Ther.* 2011;22(9):1143-1153.

59. McCarty DM, et al. Adeno-associated virus terminal repeat (TR) mutant generates self-complementary vectors to overcome the rate-limiting step to transduction in vivo. *Gene Ther.* 2003;10(26):2112-2118.

60. McCarty DM, et al. Self-complementary recombinant adeno-associated virus (scAAV) vectors promote efficient transduction independently of DNA synthesis. *Gene Ther.* 2001;8(16):1248-1254.

61. Gray SJ, et al. Production of recombinant adeno-associated viral vectors and use in in vitro and in vivo administration. *Current protocols in neuroscience / editorial board, Jacqueline N Crawley [et al].* 2011;Chapter 4:Unit 4.17.

62. Bailey RM, et al. Comparison of high-dose intracisterna magna and lumbar puncture intrathecal delivery of AAV9 in mice to treat neuropathies. *Brain Res.* 2020;1739:146832.

63. Chen X, et al. Pre-clinical Gene Therapy with AAV9/AGA in Aspartylglucosaminuria Mice Provides Evidence for Clinical Translation. *Mol Ther.* 2020;29(3):989-1000.

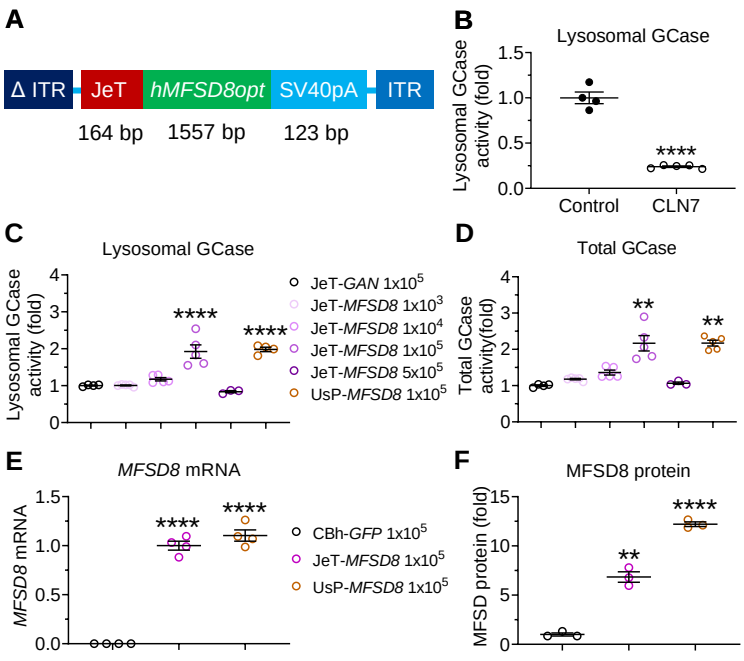

Figure 1. AAV2/*MFSD8* vector construct expressing human *MFSD8* (A) and its rescue of lysosomal function in primary fibroblasts from CLN7 patient (B-H). (A) Schematic diagram of AAV2/*MFSD8* construct comprising a mutant AAV2 inverted terminal repeat (ITR) with the D element deleted (Δ ITR), the JeT promoter, the human *MFSD8* codon-optimized coding sequence (*hMFSD8opt*), the synthetic polyadenylation SV40pA signal, and WT AAV2 ITR. (**B**) Lysosomal beta-glucocerebrosidase (GCase) activity (n=4-5) was measured in fibroblasts from age-matched healthy control and CLN7 patient. GCase activity was normalized to the cell volume. **(C-D)** Lysosomal and total GCase activity (n=3-5) was measured following AAV2-mediated transduction of JeT-*GAN* (negative control), JeT-*MFSD8* (therapeutic transgene at increasing doses), or UsP-*MFSD8* (therapeutic transgene with stronger promotor). The fold differences in lysosomal (**C**) and total (**D**) GCase activity were normalized to the cell volume and to cohorts transfected with JeT-*GAN*. In **E** and **F**, *MFSD8* mRNA and MFSD8 protein (n=3-4) were assayed following AAV2-mediated transduction of CBh-*GFP* (negative control), JeT-*MFSD8*, or UsP-*MFSD8.* A ROUT test was used first to remove any outlier. All data in **B-F** are presented as mean ± SEM with the scatter plot representing measurements from individual culture wells. Data sets that passed tests for normality or homogeneity of variance were analyzed using unpaired t-test or one-way ANOVA with α set at 0.05 and Dunnett's correction for relevant pairwise comparisons. Data sets that did not pass tests for normality or homogeneity of variance were analyzed using Kruskal-Wallis test with α set at 0.05 and Dunn's correction for relevant pairwise comparisons. **p<0.01 and ****p<0.0001 compared to control.

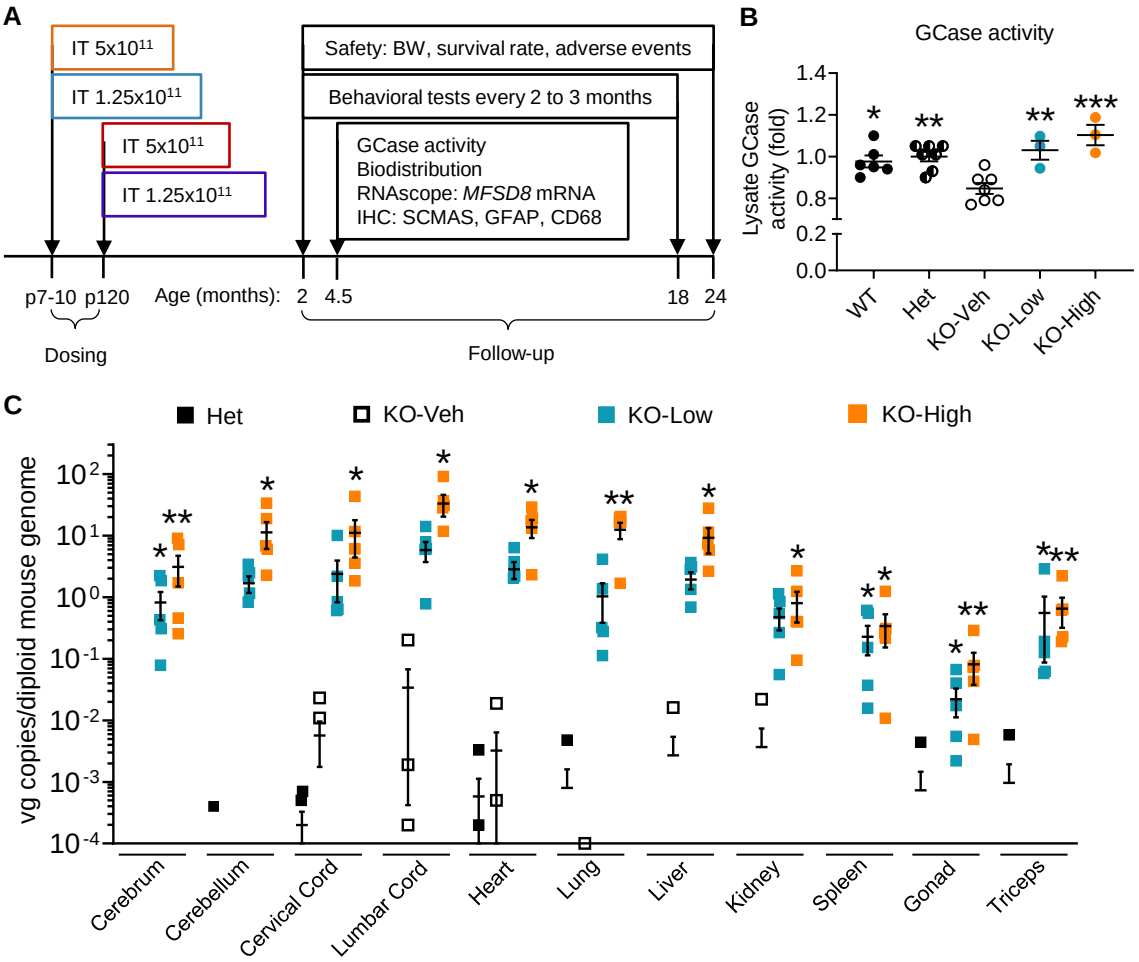

Figure 2 . The experimental design for in vivo efficacy study (A), GCase activity in mouse brain lysate (B), and vector biodistribution in central and periphery organs (C). In **A**, high ($5x10^{11}$ vg/mouse) or low ($1.25x10^{11}$ vg/mouse) dose of AAV9/*MFSD8* vector was administered intrathecally to balanced male and female mice at postnatal day p7-10 (pre-symptomatic) or p120 (early-symptomatic). Study readouts at each time point at specified age are listed from left to right. In **B**, GCase activity was measured in brain lysates of mice treated at p7-10 and harvested at 4.5 months old (n=3-7). In **C**, Vector biodistribution was measured in central and periphery organs from mice treated at p7-10 and harvested at 4.5 months old (n=3-7). A ROUT test was used first to remove any outlier. Data in **B** were normalized to Het mice. All data in B and C were presented as mean ± SEM with the scatter plot representing measurements from individual mice. Data sets in **B** and **C** that passed tests for normality or homogeneity of variance were analyzed using one-way ANOVA with α set at 0.05 and Dunnett's correction for relevant pairwise comparisons. Data sets that did not pass tests for normality or homogeneity of variance were analyzed using Kruskal-Wallis test with α set at 0.05 and Dunn's correction for relevant pairwise comparisons. *p<0.05, **p<0.01, and ***p<0.001 compared to KO-Veh. KO-Veh, KO mice receiving vehicle; KO-Low, KO mice receiving low dose; KO-High, KO mice receiving high dose; vg, vector genome; BW, body weight; IHC, immunohistochemistry; SCMAS, subunit c of mitochondrial ATP synthase; GFAP, Glial fibrillary acidic protein; CD68, Cluster of Differentiation 68.

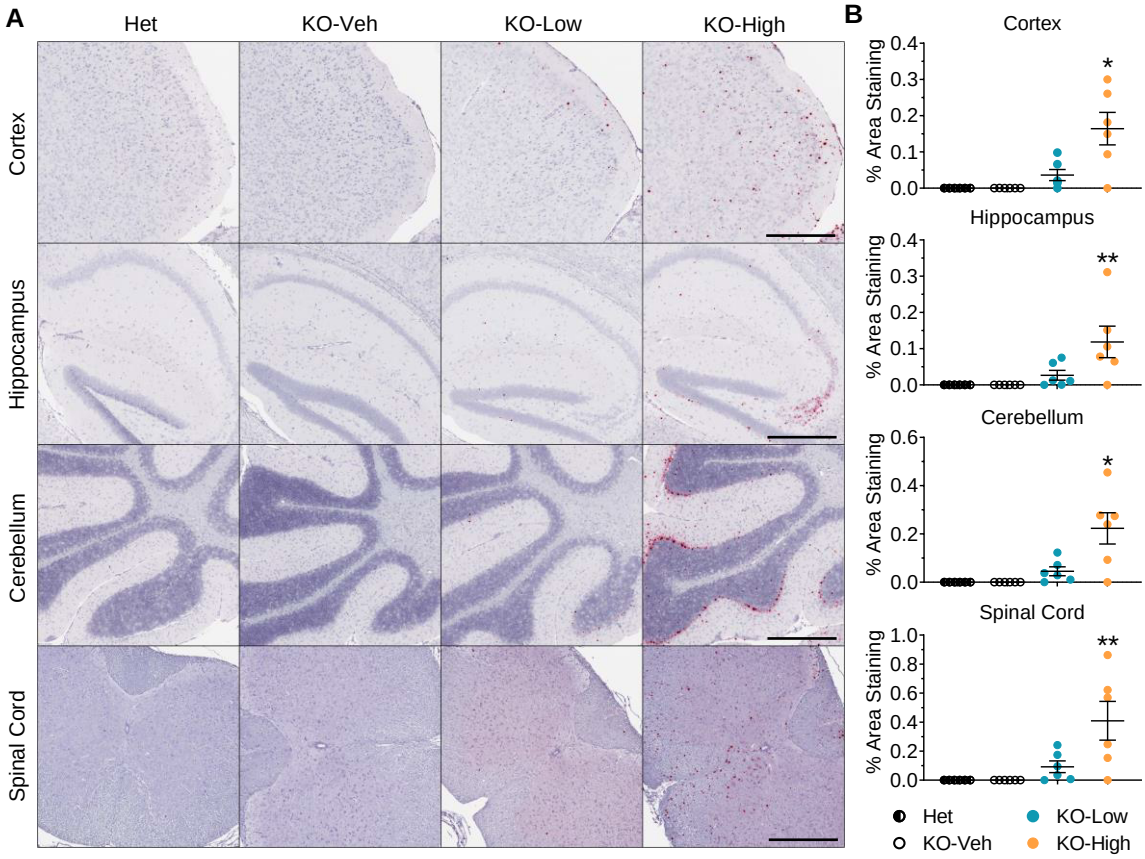

Figure 3. AAV9/*MFSD8* gene therapy (GT) dose-dependently induces *hMFSD8opt* mRNA expression in the CNS of *Mfsd8*$^{-/-}$ (KO) mice. High ($5x10^{11}$ vg/mouse) or low ($1.25x10^{11}$ vg/mouse) dose of AAV9/*MFSD8* vector was administered intrathecally to balanced male and female mice at postnatal day p7-10. At 4.5 months old, mouse brain and spinal cord were harvested for RNAscope staining to detect *hMFSD8opt* mRNA (**A**). Histology images with 1 section/animal were digitized with a ScanScope slide scanner and analyzed using custom analysis settings in HALO™ Image Analysis Platform. Results are presented as % area staining positive for *hMFSD8opt* mRNA by tissue region (**B**). A ROUT test was used first to remove any outlier. Each data point represents measurement from an individual animal (n=5-6), with lines representing the mean measurement ± SEM. Data sets that passed tests for normality or homogeneity of variance were analyzed using one-way ANOVA with α set at 0.05 and Dunnett's correction for relevant pairwise comparisons. Data sets that did not pass tests for normality or homogeneity of variance were analyzed using Kruskal-Wallis test with α set at 0.05 and Dunn's correction for relevant pairwise comparisons. *p<0.05 and **p<0.01 compared to KO-Veh. KO-Veh, KO mice receiving vehicle; KO-Low, KO mice receiving low dose; KO-High, KO mice receiving high dose. Scale bars for Cortex**,** Hippocampus, Cerebellum, and Spinal cord, 500µm.

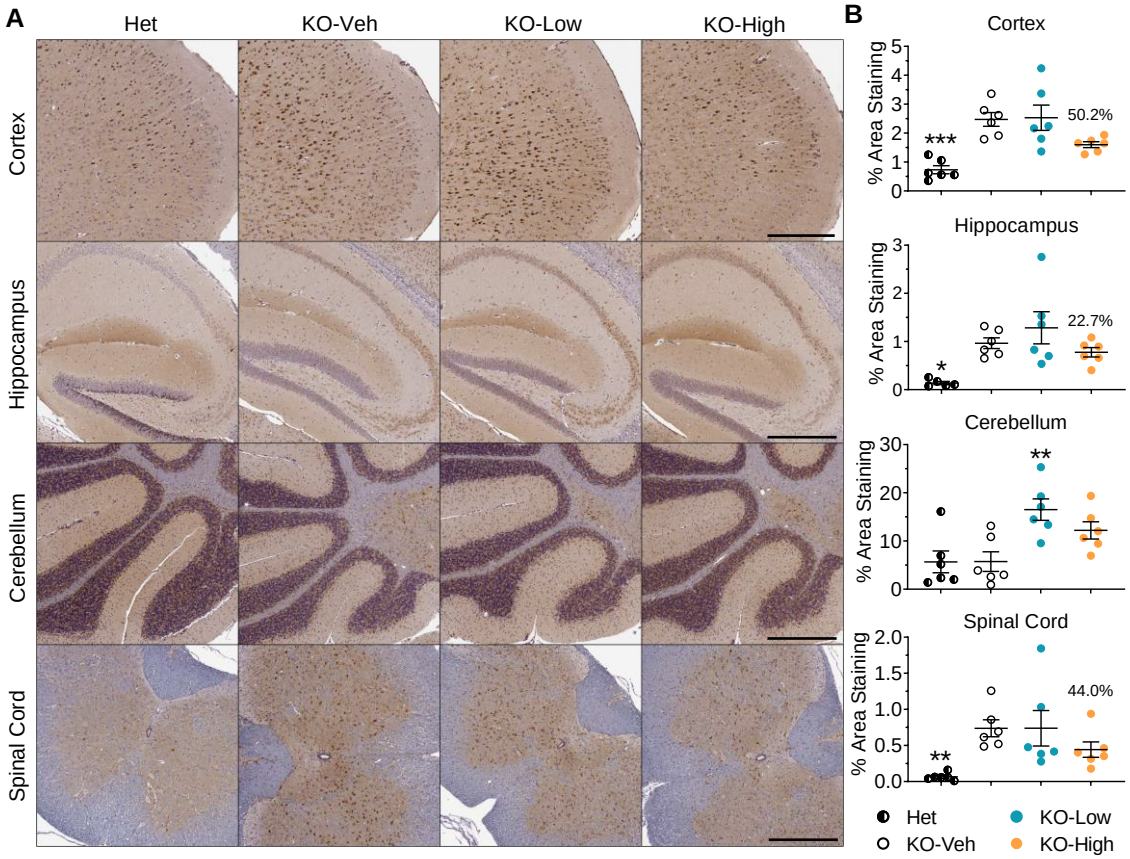

Figure 4. High dose of AAV9/*MFSD8* GT tends to ameliorate SCMAS accumulation in the brain and spinal cord of *Mfsd8*$^{-/-}$ (KO) mice. High ($5x10^{11}$ vg/mouse) or low ($1.25x10^{11}$ vg/mouse) dose of AAV9/*MFSD8* vector was administered intrathecally to balanced male and female mice at postnatal day p7-10. At 4.5 months old, mouse brain and spinal cord were harvested for IHC staining to detect SCMAS (**A**). Histology images with 1 section/animal were digitized with a ScanScope slide scanner and analyzed using custom analysis settings in HALO™ Image Analysis Platform. Results are presented as % area staining positive for SCMAS by tissue region (**B**). The % value above the KO-high group (**B**) indicate % reduction of SCMAS accumulation (Supplemental Table 1). A ROUT test was used first to remove any outlier. Each data point represents measurement from an individual animal (n=5-6), with lines representing the mean measurement ± SEM. Data sets that passed tests for normality or homogeneity of variance were analyzed using one-way ANOVA with α set at 0.05 and Dunnett's correction for relevant pairwise comparisons. Data sets that did not pass tests for normality or homogeneity of variance were analyzed using Kruskal-Wallis test with α set at 0.05 and Dunn's correction for relevant pairwise comparisons. *p<0.05, **p<0.01 and ***p<0.001 compared to KO-Veh**.** KO-Veh, KO mice receiving vehicle; KO-Low, KO mice receiving low dose; KO-High, KO mice receiving high dose; IHC, immunohistochemistry; SCMAS, subunit c of mitochondrial ATPase synthesis. Scale bar for Cortex, 300μm; Scale bars for Hippocampus, Cerebellum, and Spinal cord, 500μm.

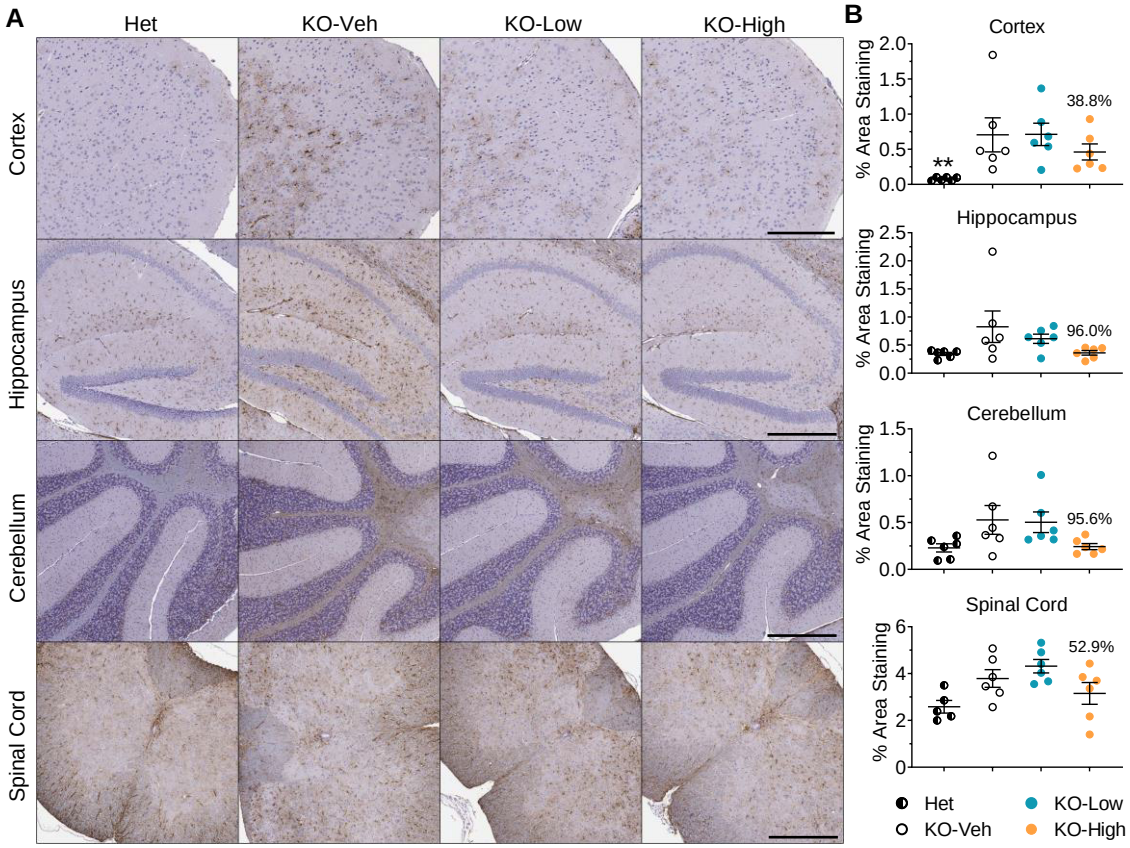

Figure 5. High dose of AAV9/*MFSD8* GT tends to decrease GFAP immunoreactivity in the brain and spinal cord of *Mfsd8*$^{-/-}$ (KO) mice. High (5x10^{11} vg/mouse) or low (1.25x10^{11} vg/mouse) dose of AAV9/*MFSD8* vector was administered intrathecally to balanced male and female mice at postnatal day p7-10. At 4.5 months old, mouse brain and spinal cord were harvested for IHC staining to detect GFAP (**A**). Histology images with 1 section/animal were digitized with a ScanScope slide scanner and analyzed using custom analysis settings in HALO™ Image Analysis Platform. Results are presented as % area staining positive for GFAP by tissue region (**B**). The % value above the KO-high group (B) indicate % reduction of GFAP accumulation (Supplemental Table 1). A ROUT test was used first to remove any outlier. Each data point represents measurement from an individual animal (n=5-6), with lines representing the mean measurement ± SEM. Data sets that passed tests for normality or homogeneity of variance were analyzed using one-way ANOVA with α set at 0.05 and Dunnett's correction for relevant pairwise comparisons. Data sets that did not pass tests for normality or homogeneity of variance were analyzed using Kruskal-Wallis test with α set at 0.05 and Dunn's correction for relevant pairwise comparisons. **p<0.01 compared to KO-Veh. KO-Veh, KO mice receiving vehicle; KO-Low, KO mice receiving low dose; KO-High, KO mice receiving high dose; IHC, immunohistochemistry; GFAP, glial fibrillary acidic protein. Scale bar for Cortex, 300μm; Scale bars for Hippocampus, Cerebellum, and Spinal cord, 500μm.

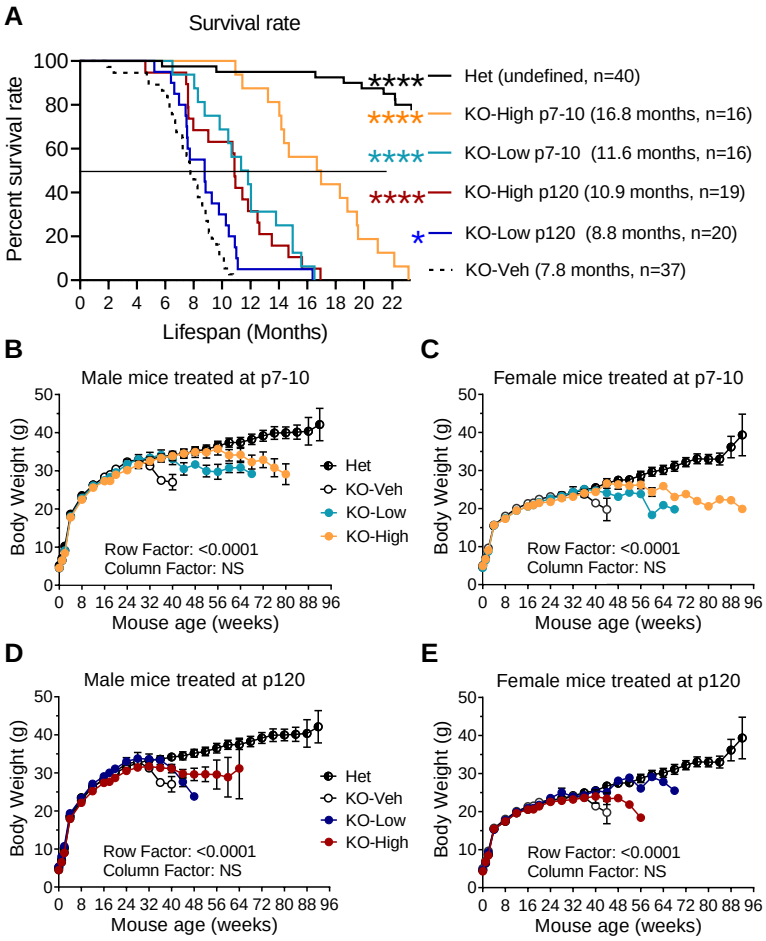

Figure 6. AAV9/*MFSD8* GT improves survival rate, extends median lifespan, (A) and maintains normal body weight longer in *Mfsd8*$^{-/-}$ (KO) mice (B-E). High ($5x10^{11}$ vg/mouse) or low ($1.25x10^{11}$ vg/mouse) dose of AAV9/*MFSD8* vector was administered intrathecally to balanced male and female mice at postnatal day p7-10 or p120. (**A**) Kaplan-Meier survival curve shows the survival over time with median survival and mice number enrolled in parenthesis. Data were compared with Log-rank (Mantel-Cox) test. *p<0.05, ****p<0.0001 compared to KO-Veh. (**B-F)** Body weight of animal treated at p7-10 (**B-C**) or p120 (**E-F**). All data in **B-F** are presented as mean ± SEM (n=16-40) and Two-way ANOVA with repeated measures was used for significant analyses. KO-Veh, KO mice receiving vehicle; KO-Low, KO mice receiving low dose; KO-High, KO mice receiving high dose.

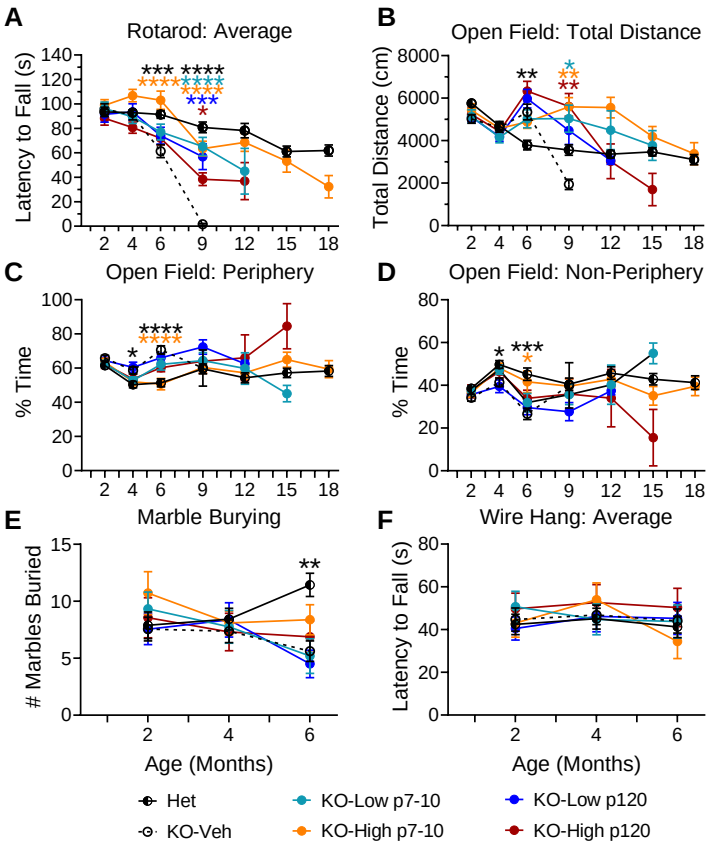

Figure 7. AAV9/*MFSD8* GT restores impaired behavioral phenotypes in *Mfsd8*$^{-/-}$ mice. High ($5x10^{11}$ vg/mouse) or low ($1.25x10^{11}$ vg/mouse) dose of AAV9/*MFSD8* vector was administered intrathecally to balanced male and female mice at postnatal day p7-10 or p120. The mice were allowed to survey a Rotarod (**A**), and Open Field (**B-D**), Marble Burying (**E**), and Wire Hang (**F**) tests. All data are presented as mean ± SEM (n=16-40). Data sets of each timepoint that passed tests for normality or homogeneity of variance were analyzed using one-way ANOVA with α set at 0.05 and Dunnett's correction for relevant pairwise comparisons. Data sets that did not pass tests for normality or homogeneity of variance were analyzed using Kruskal-Wallis test with α set at 0.05 and Dunn's correction for relevant pairwise comparisons. *p<0.05, **p<0.01, ***p<0.001, ****p<0.0001 compared to KO-Veh. KO-Veh, KO mice receiving vehicle; KO-Low, KO mice receiving low dose; KO-High, KO mice receiving high dose.

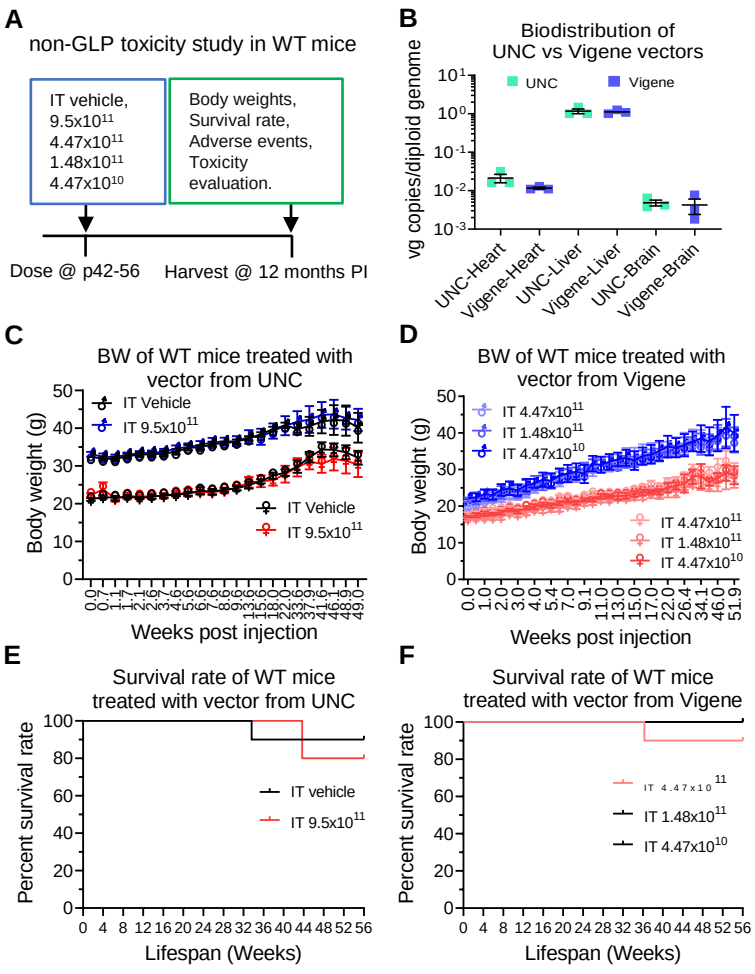

Figure 8. AAV9/*MFSD8* GT does not significantly affect body weight or survival rate of WT mice in non-GLP toxicity study. Panel **A** shows the experimental design of the non-GLP toxicity study in WT mice. Panel **B** shows the *in vivo* equivalence of preclinical lots of AAV9/*MFSD8* vectors from UNC and Vigene. WT Mice (n=3) in each group were injected with the vector via tail vein in a 200 µL bolus of 2×10^{11} vg/mouse. Mouse heart, liver, and brain were harvested a week later for biodistribution analysis. Data sets that passed tests for normality or homogeneity of variance were analyzed using unpaired t test with α set at 0.05. Data sets that did not pass tests for normality or homogeneity of variance were analyzed using Mann-Whitney test with α set at 0.05. No significance was observed. Panels **C** and **D** show the body weight of WT mice (n=5/group/sex) treated with vector from UNC (**C**) or Vigene (**D**). Two-way ANOVA with repeated measures was used for statistical analysis and no interaction significance was observed. All data in **B-D** are presented as mean ± SEM. Panels **E** and **F** show the survival rate of WT mice (n=5/group/sex) treated with vector from UNC (**E**) or Vigene (**F**). Data showing in Kaplan-Meier survival curve were compared with Log-rank (Mantel-Cox) test. No significance was observed.

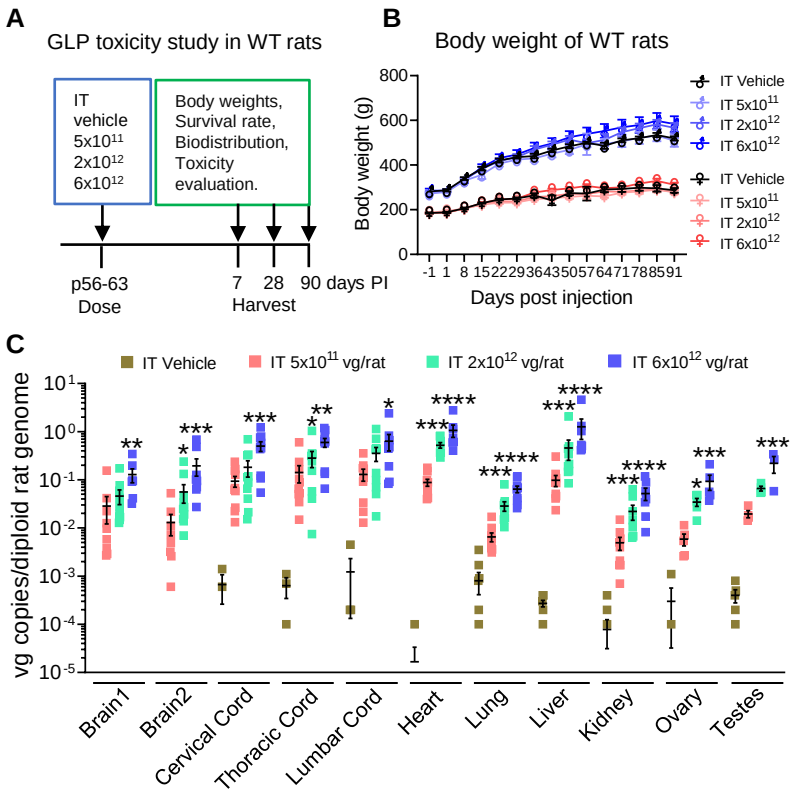

Figure 9 . AAV9/*MFSD8* GT dose-dependently increases *MFSD8* biodistribution in all rat organs tested (C) but does not significantly affect body weight (B) or cause severe adverse effects in WT rats in a GLP toxicity study (A). Panel **A** shows the experimental design of the GLP toxicity study in WT rats. Panel **B** shows the body weight of WT rats treated with vector from Vigene. Two-way ANOVA with repeated measures was used for statistical analysis and no interaction significance was observed. Panel **C** shows the *MFSD8* biodistribution of organs harvested at 28 days following the administration of AAV9/*MFSD8* vector. Data sets that passed tests for normality or homogeneity of variance were analyzed using one-way ANOVA with α set at 0.05 and Dunnett's correction for relevant pairwise comparisons. Data sets that did not pass tests for normality or homogeneity of variance were analyzed using Kruskal-Wallis test with α set at 0.05 and Dunn's correction for relevant pairwise comparisons. All data in **B** and **C** are presented as mean ± SEM (n=5/group/sex).